Hawkins, J., Parson, L., Allan, J., et al., 1994
Proceedings of the Ocean Drilling Program, Scientific Results, Vol. 135

32. EXPERIMENTAL PHASE RELATIONS OF BASALTIC ANDESITE FROM HOLE 839B UNDER HYDROUS AND ANHYDROUS CONDITIONS[1]

Glenn A. Gaetani,[2] Timothy L. Grove,[2] and Wilfred B. Bryan[3]

ABSTRACT

Experimental phase relations were used to assess the role of volatiles and crustal level fractional crystallization in the petrogenesis of lavas from Hole 839B in the central Lau Basin. Melting experiments were performed on Sample 135-839B-15R-2, 63–67 cm, at 1 atm, anhydrous, and 2 kbar, H_2O-saturated (~6 wt% H_2O in the melt) to determine the influence of variable pressure and H_2O content on phase appearances, mineral chemistry, and liquid line of descent followed during crystallization. The effects of H_2O are to depress the liquidus by ~100°C, and to suppress crystallization of plagioclase and orthopyroxene relative to olivine and high-Ca clinopyroxene. At 1 atm, anhydrous, olivine and plagioclase coexist near the liquidus, whereas orthopyroxene and then clinopyroxene appear with decreasing temperature. Crystallization of 50 wt% produces a residual liquid that is rich in FeO^* (10.8 wt%) and poor in Al_2O_3 (13.6 wt%). At 2 kbar, H_2O-saturated, the liquidus phases are olivine and chromian spinel, with high-Ca clinopyroxene appearing after ~10% crystallization. Plagioclase saturation is suppressed until ~20% crystallization has occurred. The residual liquid from 35 wt% crystallization is rich in Al_2O_3 (17.4 wt%), and poor in MgO (4.82 wt%); it contains moderate FeO^* (8.2 wt%), and resembles the low-MgO andesites recovered from Hole 839B. On the basis of these experiments we conclude that the primitive lavas recovered from Hole 839B have experienced crystallization along the Ol + Cpx saturation boundary, under hydrous conditions (an ankaramitic liquid line of descent), and variable amounts of olivine and chromian spinel accumulation. The low-MgO andesites from Hole 839B are the products of hydrous fractional crystallization, at crustal pressures, of a parent magma similar to basaltic andesite Sample 135-839B-15R-2, 63–67 cm.

INTRODUCTION

This paper presents the results of melting experiments designed to identify conditions of crystallization that led to the compositional variations in lavas recovered from Ocean Drilling Program (ODP) Hole 839B in the central Lau Basin, and to estimate their pre-eruptive H_2O contents. These lavas display the strongest affinity to island arc basalts (IAB), in terms of large ion lithophile element (LILE) enrichments and high field strength element (HFSE) depletions (Perfit et al., 1980), of any samples recovered from backarc sites during Leg 135. Hole 839B sampled highly vesicular (up to 40 vol% vesicles) extrusive flows and pillows erupted at the Eastern Lau Spreading Center (ELSC) at approximately 1 Ma. The major element systematics of these samples differ from other backarc lavas recovered during Leg 135; they display a positive correlation between SiO_2 and Al_2O_3, indicating a lack of plagioclase control during fractional crystallization (Parsons, Hawkins, Allan, et al., 1992).

Liquid lines of descent were determined at 1 atm, anhydrous, and 2 kbar, H_2O-saturated (~6 wt% H_2O in the melt), to examine the influence of variable H_2O contents on primitive Hole 839B magmas crystallizing at crustal pressures. The addition of H_2O produces distinctive shifts in the position of the high-Ca clinopyroxene (Cpx) + plagioclase (Pl) + olivine (Ol) and clinopyroxene + plagioclase + orthopyroxene (Opx) saturation boundaries. This leads to an interval of crystallization of high-Ca clinopyroxene and olivine, with a small amount of chromian spinel, similar to the crystallization sequence observed in the lavas recovered from Hole 839B. Crystallization of 35 wt% produces a residual liquid that is enriched in silica and plagioclase relative to the product of anhydrous crystallization, because of the suppression of plagioclase and orthopyroxene crystallization and the early appearance of high-Ca clinopyroxene. The evolved liquids produced in our 2 kbar, H_2O-saturated experiments resemble the andesites recovered from the lower portion of Hole 839B in that they have high Al_2O_3, moderate CaO, and low MgO; however, they are poorer in FeO^*.

EXPERIMENTAL AND ANALYTICAL METHODS

Starting Materials

The starting material for all experiments was natural basaltic andesite Sample 135-839B-15R-2, 63–67 cm (53.3 wt% SiO_2) rock powder produced by grinding in a Spex shatterbox. This sample was chosen to be representative of the Unit 1 lavas recovered from the upper portion of Hole 839B. These lavas contain primarily olivine and high-Ca clinopyroxene phenocrysts; they are characterized by relatively low Na_2O (~1.4 wt%) and Al_2O_3 (~15 wt%) contents (Parsons, Hawkins, Allan, et al., 1992). The starting material for the 1 atm experiments was prepared by pressing pellets from 80 to 100 mg of powder, using elvanol as a binder. Pellets were then sintered onto FePt alloy loops, fabricated to minimized Fe-exchange with the sample (Grove, 1981).

1-atm Experiments

Experiments at 1 atm were performed by suspending pellets of rock powder on FePt alloy loops in the hot spot of a Deltech DT31VT vertical quenching furnace. The fugacity of oxygen was controlled near the fayalite-magnetite-quartz (FMQ) oxygen buffer using a CO_2-H_2 gas mixture, and was monitored using a solid ZrO_2-CaO electrolyte oxygen sensor calibrated against the Fe-FeO, Ni-NiO, and Cu-Cu_2O buffers. Volatilization of Na from the sample during the experiment was minimized through the use of low gas flow rates and large sample sizes (Tormey et al., 1987). Temperature was monitored using Pt-$Pt_{90}Rh_{10}$ thermocouples, calibrated against the melting point of NaCl, Au, and Pd on the IPTS 1968 temperature scale (Biggar, 1972). Experiments were terminated by quenching in H_2O.

[1] Hawkins, J., Parson, L., Allan, J., et al., 1994. *Proc. ODP, Sci. Results,* 135: College Station, TX (Ocean Drilling Program).

[2] Department of Earth, Atmospheric, and Planetary Sciences, Massachusetts Institute of Technology, Cambridge, MA 02139, U.S.A.

[3] Woods Hole Oceanographic Institute, Woods Hole, MA 02543, U.S.A.

2-kbar Experiments

Experiments at 2 kbar were performed using TZM (titanium-zirconium-molybdenum) and ZHM (zirconium-hafnium carbide-molybdenum) rapid quench cold-seal pressure vessels. Rock powder was placed in a noble metal capsule that was welded closed on the bottom and crimped on the top. This capsule was placed in a larger noble metal capsule along with H_2O and Ni-NiO buffers to control the fugacity of oxygen during the experiment. The outer capsule was then sealed with an arc welder and placed in the bottom of the pressure vessel. The vessel was pumped to ~1.5 kbar at room temperature, using a mixture of Ar and CH_4 gases as a pressure medium, and placed in a Deltech DT31VT vertical furnace with the sample located in the hotspot. The furnace temperature was brought up to experimental conditions over approximately 1 hr. Pressure was allowed to increase with increasing temperature until the vessel reached 2 kbar, after which it was maintained by bleeding off small amounts of gas. Experiments were terminated by removing the pressure vessel from the furnace and inverting it, so that the sample slid to the cold end and was rapidly quenched against the cooling head. Experiments were judged successful if the capsule contained H_2O at the end of the experiment, buffers contained both Ni and NiO, and the glass was free of quench growth.

The element Au was used as capsule material for experiments performed at temperatures of 1050°C or below. The use of Au limits the range of temperatures that can be investigated (the 1-atm melting point of Au is 1064°C), but it also minimizes the problem of iron loss to the sample container. Experiments above 1050°C were performed using $Ag_{70}Pd_{30}$ inner and $Au_{80}Pt_{20}$ outer capsules. Oxygen buffers consisted of a mixture of Ni and NiO powder in a Pt or $Ag_{70}Pd_{30}$ capsule. Buffer capsules were left unsealed so that the Ni-NiO mixture remained in contact with the same atmosphere as the experimental charge. Temperature was monitored using Pt-$Pt_{90}Rh_{10}$ thermocouples, calibrated as outlined above for the 1-atm experiments, located in a well on the outside of the pressure vessel. The temperature difference between the position of the thermocouple and the sample was calibrated several times, and reported experimental temperatures are precise to within ±7°C. Pressure was monitored with a Heise gauge.

Analytical Methods

Experimentally produced minerals and glasses, and phenocrysts from Hole 839B lavas were analyzed using the MIT 4-spectrometer JEOL 733 superprobe. On-line data reduction consisted of the matrix corrections of Bence and Albee (1968), with the modifications of Albee and Ray (1970). A 10-nA beam current and 15-kV accelerating potential were used for all analyses. Beam widths were 20 µm for hydrous glasses, 10 µm for anhydrous glasses, and ~3 µm for crystalline phases. Counting times were 5 s for Na, and up to 40 s for all other elements.

Analyses of experimentally produced crystalline phases, with the exception of chromian spinel, were performed on rims directly adjacent to glass. This was done to avoid analyzing any unreacted cores remaining from the starting materials. The presence of residual cores is most pronounced in low temperature, anhydrous experiments where the melt fraction is relatively small (~50 wt%) and diffusion rates were comparatively slow. Cores were small or absent in hydrous experiments. The presence of unreacted cores indicates that bulk equilibrium was not achieved; however, mineral-melt exchange K_D's (discussed below) indicate that a close approach to surface equilibrium was attained.

EXPERIMENTAL RESULTS

1 atm, Anhydrous

At 1 atm, under anhydrous conditions, chromian spinel is the liquidus phase, followed by an assemblage of olivine (Fo_{85}), plagioclase (An_{87}), and chromian spinel (Table 1). Orthopyroxene coexists with olivine and plagioclase at 1180°C, and the melt reaches the "olivine out" reaction point (Grove and Baker, 1984) at 1170°C, when the melt saturates with high-Ca clinopyroxene. The melt remains on the Cpx + Opx + Pl saturation boundary to the lowest temperature investigated (1150°C).

Table 1. Experimental conditions and phase assemblages.

Run no.	Temperature (°C)	log fO_2	Duration (hr)	Run products	Phase proportions (wt%)
1 atm, anhydrous					
23	1210	–8.52	27	Gl, Sp	100.0 : Tr
22	1190	–8.71	58	Gl, Pl, Ol, Sp	92.2 : 4.3 : 3.5 : Tr
21	1180	–8.86	76	Gl, Opx, Pl, Ol	81.7 : 5.7 : 10.3 : 2.3
19	1170	–8.94	72	Gl, Cpx, Opx, Pl, Ol	69.7 : 1.2 : 13.1 : 16.0 : Tr
17	1160	–9.17	72	Gl, Cpx, Opx, Pl	51.0 : 8.6 : 15.1 : 25.3
8	1150	–9.06	72	Gl, Cpx, Opx, Pl	49.9 : 7.9 : 16.8 : 25.4
2 kbar, water saturated					
24	1100	—	3	Gl, Ol, Sp	99.0 : 1.0 : Tr
18[a]	1075	—	13	Gl, Ol, Sp	96.0 : 4.0 : Tr
12	1050	—	24	Gl, Cpx, Ol, Sp	88.6 : 5.7 : 5.7 : Tr
7[b]	1035	—	24	Gl, Cpx, Ol, Sp	86.7 : 7.1 : 6.2 : Tr
4	1035	—	24	Gl, Cpx, Ol, Sp	83.2 : 10.2 : 6.6 : Tr
5	1020	—	24	Gl, Cpx, Ol, Pl, Sp	79.7 : 12.7 : 7.1 : 0.5 : Tr
6	1005	—	24	Gl, Cpx, Ol, Pl, Sp	65.4 : 15.8 : 9.1 : 9.7 : Tr

Notes: Tr = trace, Gl = glass, Sp = chromian spinel, Pl = plagioclase, Ol = olivine, Opx = orthopyroxene, and Cpx = high-Ca clinopyroxene.
[a] fO_2< NiNiO.
[b] ZHM pressure vessel.

Melt compositions display the variations typical of basalt crystallization under anhydrous conditions (Table 2). CaO, Al_2O_3, and MgO all decrease monotonically with decreasing melt fraction (F), because of the crystallization of plagioclase and ferromagnesian silicates, whereas SiO_2, Na_2O, K_2O, TiO_2 and FeO^* increase. The result of ~50% crystallization (by weight) is an iron-rich (10.8 wt% FeO^*), alumina-poor (13.6 wt%) basaltic andesite (54.9 wt% SiO_2).

The composition of experimentally produced pyroxenes are shown in Figure 1 and reported in Table 2. The experiment performed at 1180°C contained orthopyroxene, and those from 1170°C to 1150°C contained coexisting low- and high-Ca pyroxenes. All high-Ca pyroxene compositions plot in the augite field of the pyroxene quadrilateral (Poldervaart and Hess, 1951). Olivine compositions range from Fo_{85} to Fo_{81}, and plagioclase compositions range from An_{87} to An_{77} (Table 2). The mean Fe-Mg mineral-melt exchange K_D's are 0.30 ± 0.01 for olivine, 0.25 ± 0.03 for orthopyroxene, and 0.26 ± 0.01 for high-Ca pyroxene. The mean plagioclase-melt Ca-Na exchange K_D is 1.38 ± 0.21. These K_D's are similar to the experimentally determined values of 0.30 for olivine (Roeder and Emslie, 1970), 0.23 for pyroxene (Grove and Bryan, 1983), and 1.13 for plagioclase (Grove et al., 1990), indicating a close approach to equilibrium between the surface of the crystals and the surrounding melt.

2 kbar, H_2O Saturated

The liquidus phases at 2 kbar, H_2O-saturated, are olivine (Fo_{86}) and chromian spinel. The highest temperature experiment contained only ~1% olivine phenocrysts, implying that 1100°C is close to the liquidus temperature (Table 1). This indicates that the liquidus has been depressed by ~100°C relative to anhydrous conditions. High-Ca clinopyroxene (endiopside) joins the crystallizing assemblage between 1075° and 1050°C, and becomes the dominant crystallizing phase until the melt becomes saturated with calcic plagioclase (An_{94}) at 1020°C.

The variations in melt composition produced at 2 kbar with ~6 wt% H_2O in the melt are distinct from those produced at 1 atm, anhydrous (Table 3). SiO_2, Na_2O, TiO_2, and K_2O all increase with decreasing F, whereas MgO decreases, as was the case in the anhydrous experiments. The major difference caused by H_2O saturation at 2 kbar is that SiO_2 increases and MgO decreases more rapidly in the residual liquid. In contrast with anhydrous crystallization, FeO^* decreases slightly with decreasing F. The behavior of CaO and Al_2O_3 are controlled by the crystallization of high-Ca clinopyroxene and plagioclase. CaO in-

Table 2. Electron microprobe analyses of run products from 1 atm, anhydrous experiments.

Run no.	Phase	Analyses (N)	SiO_2	TiO_2	Al_2O_3	Cr_2O_3	FeO*	MnO	MgO	CaO	Na_2O	K_2O	P_2O_5	Total
23	Gl	10	53.3(2)	0.60(3)	15.16(8)	0.05(3)	8.85(8)	0.22(2)	9.36(5)	11.3(1)	1.48(5)	0.30(2)	0.11(3)	100.73
22	Gl	10	53.7(2)	0.64(2)	14.81(9)	0.06(3)	8.9(1)	0.13(6)	8.31(4)	11.45(9)	1.47(4)	0.30(1)	0.15(1)	99.92
	Ol	5	39.4(2)	0.00(0)	0.05(1)	0.07(0)	14.3(1)	0.26(2)	45.6(5)	0.31(1)	—	—	—	99.99
	Pl	5	47.9(5)	—	31.9(12)	—	1.1(3)	—	0.9(4)	17.1(5)	1.36(6)	0.07(1)	—	100.33
21	Gl	10	53.5(1)	0.73(3)	14.26(7)	0.07(3)	9.4(1)	0.19(3)	7.91(9)	11.5(2)	1.55(6)	0.30(1)	0.16(2)	99.57
	Opx	7	55.8(3)	0.11(2)	1.0(2)	0.4(1)	9.9(3)	0.23(1)	30.1(4)	2.5(1)	0.01(1)	—	—	100.05
	Ol	5	39.2(2)	0.01(1)	0.3(5)	0.07(1)	15.8(3)	0.27(3)	44.0(8)	0.5(3)	—	—	—	100.15
	Pl	7	47.9(6)	—	31.3(16)	—	1.2(6)	—	1.0(6)	16.9(5)	1.5(1)	0.05(2)	—	99.85
19	Gl	10	53.4(2)	0.87(3)	13.93(9)	0.05(2)	10.3(1)	0.24(5)	7.5(1)	11.4(1)	1.66(9)	0.36(2)	0.17(3)	99.88
	Cpx	8	52.9(4)	0.22(2)	2.5(4)	0.6(3)	6.60(3)	0.17(2)	18.5(4)	18.9(8)	0.13(2)	—	—	100.52
	Opx	7	55.7(2)	0.09(1)	1.0(1)	0.37(3)	10.8(1)	0.25(2)	29.5(4)	2.46(7)	0.02(1)	—	—	100.19
	Ol	5	39.1(4)	0.00(1)	0.07(5)	0.04(1)	17.7(1)	0.28(3)	42.6(5)	0.39(5)	—	—	—	100.18
	Pl	4	48.2(7)	—	32.2(6)	—	0.80(5)	—	0.5(1)	16.8(3)	1.7(2)	0.05(1)	—	100.25
17	Gl	10	54.2(4)	1.0(1)	13.7(1)	0.01(2)	11.2(2)	0.21(4)	6.5(1)	10.6(2)	1.9(1)	0.42(2)	0.20(1)	99.94
	Cpx	7	52.8(7)	0.27(6)	2.3(6)	0.5(2)	8.3(4)	0.24(4)	18.2(5)	17.6(7)	0.12(3)	—	—	100.33
	Opx	7	55.5(4)	0.11(1)	1.1(3)	0.32(6)	12.7(3)	0.27(1)	28.1(3)	2.49(5)	0.05(1)	—	—	100.64
	Pl	7	50.2(7)	—	30.4(7)	—	1.1(2)	—	0.5(1)	15.4(5)	2.5(2)	0.08(2)	—	100.18
8	Gl	10	54.9(4)	1.07(8)	13.6(1)	0.02(2)	10.8(3)	0.22(4)	6.3(1)	10.6(1)	1.9(1)	0.48(2)	0.19(4)	100.08
	Cpx	7	52.8(5)	0.28(4)	2.7(7)	0.5(2)	8.2(4)	0.21(3)	18.0(7)	17.8(7)	0.18(5)	—	—	100.67
	Opx	7	54.9(3)	0.17(1)	1.1(2)	0.29(5)	13.3(2)	0.28(3)	27.3(3)	2.6(2)	0.03(1)	—	—	99.97
	Pl	4	49.8(8)	—	31.0(3)	—	0.91(7)	—	0.47(4)	15.9(5)	2.3(3)	0.07(2)	—	100.45

Notes: Units in parentheses represent 1 standard deviation of least units cited, based on replicate analyses; thus, 53.3(2) should be read as 53.3 ± 0.2. Abbreviations as in Table 1, with the addition of N = number of analyses.

Table 3. Electron microprobe analyses of run products from 2 kbar, water-saturated experiments.

Run no.	Phase	Analyses (N)	SiO_2	TiO_2	Al_2O_3	Cr_2O_3	FeO*	MnO	MgO	CaO	Na_2O	K_2O	P_2O_5	Total
24	Gl	10	53.1(1)	0.63(3)	15.12(8)	0.01(2)	8.8(1)	0.18(3)	8.93(5)	11.43(9)	1.5(1)	0.27(2)	0.12(2)	93.82
	Ol	5	40.0(4)	0.02(2)	0.06(3)	0.10(2)	13.6(6)	0.24(2)	45.6(3)	0.32(2)	—	—	—	99.94
18	Gl	10	53.3(2)	0.65(2)	15.6(8)	0.07(3)	8.6(1)	0.16(2)	7.85(6)	11.76(8)	1.60(9)	0.30(2)	0.15(2)	93.73
	Ol	5	39.8(4)	0.03(2)	0.07(1)	0.11(2)	15.4(5)	0.23(3)	44.5(7)	0.29(2)	—	—	—	100.43
	Sp	5	0.06(7)	0.5(2)	12.8(23)	49.2(47)	24.9(25)	0.36(3)	10.2(4)	0.36(5)	—	—	—	98.38
12	Gl	10	54.0(2)	0.70(4)	16.9(1)	0.03(2)	8.27(7)	0.19(4)	6.66(5)	11.21(2)	1.6(1)	0.31(1)	0.14(2)	94.52
	Cpx	7	53.0(3)	0.24(2)	2.6(3)	0.79(9)	5.3(4)	0.15(3)	17.4(3)	21.5(4)	0.13(1)	—	—	101.11
	Ol	5	39.5(4)	0.01(1)	0.06(3)	0.03(2)	16.5(3)	0.25(2)	43.4(6)	0.4(2)	—	—	—	100.15
	Sp	2	0.21(3)	0.5(2)	14.7(17)	47.9(36)	25.0(10)	0.33(0)	10.2(2)	0.34(1)	—	—	—	99.18
7	Gl	10	54.0(6)	0.67(2)	17.2(2)	0.00(0)	8.2(2)	0.14(4)	6.40(7)	11.1(2)	1.8(1)	0.35(2)	0.16(1)	94.11
	Cpx	10	52.6(6)	0.26(3)	2.8(5)	0.7(1)	5.1(2)	0.15(2)	16.9(4)	21.8(3)	0.14(2)	—	—	100.45
	Ol	5	39.0(3)	0.01(1)	0.04(3)	0.02(1)	18.1(4)	0.25(2)	42.4(3)	0.27(2)	—	—	—	100.09
4	Gl	10	54.4(1)	0.70(5)	17.7(1)	0.03(2)	8.0(1)	0.22(4)	5.85(6)	10.8(1)	1.85(9)	0.34(1)	0.20(3)	92.84
	Cpx	10	52.4(4)	0.33(9)	2.9(3)	0.6(1)	6.4(9)	0.18(3)	16.9(5)	20.5(7)	0.14(2)	—	—	100.35
	Ol	5	38.9(4)	0.03(0)	0.05(2)	0.04(1)	18.5(4)	0.26(2)	42.0(3)	0.24(2)	—	—	—	100.02
5	Gl	10	54.5(3)	0.74(3)	18.18(9)	0.01(2)	8.1(2)	0.20(5)	5.49(6)	10.5(1)	1.81(8)	0.35(1)	—	93.31
	Cpx	10	52.0(4)	0.35(7)	3.2(5)	0.6(1)	6.2(7)	0.16(4)	16.2(3)	21.0(6)	0.14(2)	—	—	99.85
	Ol	5	38.6(2)	0.01(1)	0.07(7)	0.07(3)	19.3(4)	0.25(3)	41.0(4)	0.30(5)	—	—	—	99.60
	Pl	5	45.4(5)	—	33.6(7)	—	0.7(1)	—	0.2(1)	18.8(2)	0.65(5)	0.02(2)	—	99.37
	Sp	2	0.13(2)	0.5(2)	12.1(11)	47.4(45)	30.1(32)	0.33(2)	7.8(4)	0.30(3)	—	—	—	98.66
6	Gl	10	56.3(2)	0.81(3)	17.4(1)	0.05(2)	8.2(1)	0.20(5)	4.82(4)	9.5(1)	2.13(6)	0.45(3)	0.18(2)	92.57
	Cpx	10	52.3(5)	0.36(6)	2.6(7)	0.49(7)	7.2(3)	0.18(5)	16.7(6)	20.0(3)	0.16(3)	—	—	99.99
	Ol	5	38.1(2)	0.02(1)	0.05(2)	0.07(0)	21.7(2)	0.30(1)	39.0(4)	0.26(2)	—	—	—	99.50
	Pl	10	46.3(6)	—	34.1(6)	—	0.8(1)	—	0.17(3)	18.1(5)	1.1(3)	0.01(1)	—	100.58

Notes: All glass compositions are normalized to 100% on an anhydrous basis. Original unnormalized total is reported. Abbreviations are as in Table 1, with the addition of N = number of analyses.

creases with the first few percent crystallization and then decreases steadily following pyroxene saturation. Al_2O_3 increases from 15.1 to 18.2 wt%, before plagioclase saturation (at F ≈ 80 wt%), and then decreases steadily. The residual melt from ~35 wt% crystallization is a basaltic andesite (56.3 wt% SiO_2) with relatively high alumina (17.4 wt%), moderate FeO* (8.2 wt%), and relatively low MgO (4.82 wt%). It is similar in composition to andesites typically found in arc environments (e.g., Gill, 1981).

Figure 1 shows the composition of experimentally produced high-Ca pyroxenes. They are considerably more calcic than those in equilibrium with the 1 atm, anhydrous, melts. Pyroxenes from the high-temperature experiments plot in the endiopside field of the pyroxene quadrilateral, and their compositions move into the Mg-rich part of the augite field with decreasing temperature. Olivine compositions range from Fo_{86} to Fo_{76}, whereas plagioclase compositions range from An_{94} to An_{90}. The mean Fe-Mg mineral-melt exchange K_D's are 0.32 ± 0.01 for olivine and 0.26 ± 0.02 for high-Ca clinopyroxene. The mean plagioclase-melt Ca-Na exchange K_D is 4.3 ± 0.9. The values for olivine and pyroxene are again close to previously determined values; however, the plagioclase-melt K_D is lower than the value of 5.5 reported by Sisson and Grove (1993a) from their 2 kbar, H_2O-saturated experiments.

PHENOCRYST COMPOSITIONS FROM UNIT 1 LAVAS

Phenocryst compositions were analyzed by electron microprobe from thin sections of samples from Hole 839B located below (Sample 135-839B-15R-3, 72–76 cm) and above (Sample 135-839B-14R-2, 1–8 cm) Sample 135-839B-15R-2, 63–67 cm, to help constrain the petrogenesis of Unit 1 lavas (Table 4). Sample 135-839B-15R-3, 72–76 cm, contains olivine, high-Ca clinopyroxene, and chromian spinel phenocrysts, with plagioclase occurring as occasional glomerocrystic intergrowths with clinopyroxene. Sample 135-839B-14R-2,

Table 4. Electron microprobe analyses of phenocrysts from Unit 1 lavas.

Phase	Notes	Analyses (*N*)	SiO_2	TiO_2	Al_2O_3	Cr_2O_3	FeO*	MnO	MgO	CaO	Na_2O	K_2O	NiO	Total
Sample 135-839B-15R-3, 72–76 cm:														
Cpx		3	52.0(9)	0.3(1)	2.9(10)	0.7(2)	5.8(3)	0.11(3)	17.9(8)	20.4(5)	0.10(3)	—	—	100.21
		3	52.6(1)	0.26(2)	2.24(8)	0.4(1)	6.3(5)	0.14(1)	17.9(2)	19.8(5)	0.08(2)	—	—	99.72
		4	52.4(7)	0.24(8)	2.4(7)	0.5(2)	5.7(3)	0.15(3)	18.1(4)	20.4(3)	0.07(2)	—	—	99.96
	Core	2	51.9(2)	0.26(3)	3.00(7)	1.1(1)	4.88(0)	0.07(3)	17.5(1)	21.2(0)	0.11(2)	—	—	100.02
	Rim	2	52.0(8)	0.30(7)	2.70(8)	0.42(2)	6.03(8)	0.15(1)	17.9(4)	20.1(3)	0.08(1)	—	—	99.68
Ol		2	39.3(0)	0.04(1)	0.06(2)	0.07(1)	17.1(0)	0.28(0)	43.0(2)	0.24(1)	—	—	0.14(0)	100.23
	Core	2	40.1(1)	0.04(1)	0.05(1)	0.08(0)	11.3(1)	0.18(1)	47.1(1)	0.19(0)	—	—	0.33(1)	99.37
	Rim	2	40.2(0)	0.05(1)	0.05(2)	0.09(0)	13.5(8)	0.22(2)	46.1(7)	0.20(1)	—	—	0.28(2)	100.69
		2	39.2(1)	0.05(2)	0.05(1)	0.06(1)	17.5(1)	0.29(1)	42.7(2)	0.18(0)	—	—	0.12(2)	100.15
Pl	Cpx incl.	2	45.8(1)	—	33.4(2)	—	0.85(2)	—	0.19(0)	17.8(1)	1.18(1)	0.00(0)	—	99.22
		2	46.7(2)	—	33.4(1)	—	0.68(1)	—	0.21(2)	17.8(1)	1.21(4)	0.01(1)	—	100.01
	Cpx incl.	2	47.1(2)	—	33.3(1)	—	0.81(2)	—	0.23(0)	17.6(2)	1.42(6)	0.01(1)	—	100.47
		2	46.6(6)	—	33.6(1)	—	0.63(7)	—	0.19(0)	18.0(4)	1.2(1)	0.00(0)	—	100.22
Sp	Ol incl.	1	0.00	0.53	11.8	44.0	32.1	0.44	8.38	0.04	—	—	0.22	97.51
Sample 135-839B-14R-2, 1–8 cm:														
Cpx		3	52.7(3)	0.24(3)	2.2(6)	0.4(2)	6.5(4)	0.15(1)	18.2(2)	19.7(3)	0.14(1)	—	—	100.23
Opx	Rim	3	54.3(1)	0.16(1)	1.63(5)	0.15(1)	12.7(1)	0.27(1)	28.6(0)	1.97(5)	0.02(2)	—	—	99.80
Ol	Core	3	39.3(1)	0.05(2)	0.04(2)	0.07(2)	16.9(1)	0.24(2)	43.5(1)	0.19(1)	—	—	0.20(1)	100.49
Opx	Rim	3	54.1(1)	0.18(2)	1.57(9)	0.05(3)	13.8(1)	0.31(2)	27.6(1)	2.07(8)	0.04(3)	—	—	99.72
Ol	Core	3	39.1(2)	0.01(1)	0.01(1)	0.09(1)	20.4(4)	0.29(0)	41.2(4)	0.22(1)	—	—	0.16(1)	101.48
Pl		2	45.8(1)	—	33.7(2)	—	0.88(6)	—	0.15(3)	18.2(1)	1.02(2)	0.02(2)	—	99.77
		2	45.8(2)	—	34.0(0)	—	0.89(5)	—	0.17(1)	18.2(1)	1.03(1)	0.03(3)	—	100.12
	Core	2	45.7(1)	—	34.2(1)	—	0.70(4)	—	0.15(1)	18.5(2)	0.94(4)	0.02(0)	—	100.21
	Rim	2	51.4(2)	—	30.2(0)	—	1.03(0)	—	0.16(2)	14.5(1)	3.17(5)	0.02(1)	—	100.48
Sp	Ol incl.	1	0.12	0.31	9.32	52.4	28.5	0.23	8.14	0.04	—	—	0.16	99.22
	Ol incl.	1	0.09	0.47	13.5	43.5	31.8	0.21	8.29	0.05	—	—	0.10	98.01

Notes: Abbreviations as in Table 1, with the addition of *N* = number of analyses and incl. = inclusion.

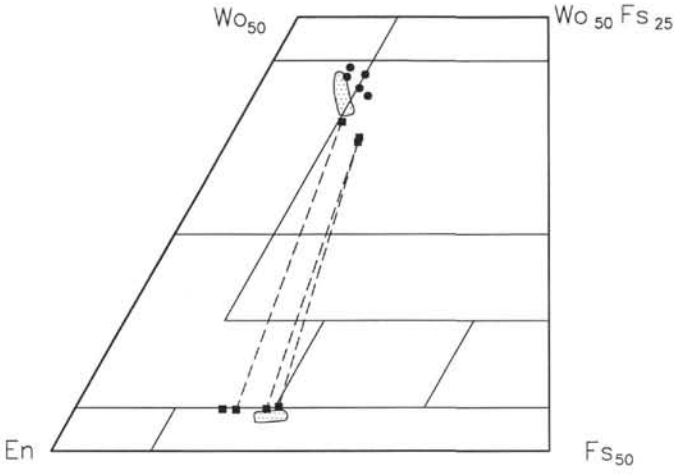

Figure 1. Composition of pyroxenes produced in anhydrous (filled squares) and water-saturated (filled circles) experiments, and phenocrysts from Hole 839B lavas (shaded fields) projected onto the Wo-En-Fs (molar) plane. Dashed lines connect coexisting high- and low-Ca pyroxenes.

1–8 cm, contains orthopyroxene, commonly cored by olivine, high-Ca clinopyroxene, chromian spinel, and some plagioclase.

The range of high-Ca clinopyroxene and orthopyroxene compositions found in thin section are compared with experimentally produced pyroxenes in Figure 1. The clinopyroxenes at the high-Ca end contain ~21 wt% CaO, and are similar to those produced in the 2-kbar experiments, whereas the low-Ca end of the trend, defined by an augite from Sample 135-839B-14R-2, 1–8 cm, approaches the pyroxenes from the 1-atm experiments. The orthopyroxenes are slightly less calcic than those from the 1-atm experiments, but they have similar Fe/Mg ratios. Olivine compositions in Sample 135-839B-15R-3, 72–76 cm, range from Fo_{88} (core composition) to Fo_{81}. The olivines analyzed in Sample 135-839B-14R-2, 1–8 cm (orthopyroxene cores), are Fo_{82} and Fo_{78}. The plagioclase phenocrysts analyzed in both thin sections are Ca-rich, with An_{89} in Sample 135-839B-15R-3, 72–76 cm, and An_{91} in Sample 135-839B-14R-2, 1–8 cm. One analyzed grain consists of an An_{92} core surrounded by an An_{72} rim ~10 μm wide.

DISCUSSION

Backarc basin basalts (BAB) exhibit a compositional range from MORB-like to IAB-like, and are variably enriched in alkalis and volatiles, especially H_2O (Hart et al., 1972). Experimental studies have demonstrated that the presence of H_2O changes the phase relations of basaltic magmas (e.g., Baker and Eggler, 1987). Therefore, to understand the melting and crystallization histories of BAB, knowledge of both hydrous and anhydrous phase boundaries is necessary.

The Pl-Cpx-SiO_2 pseudo-ternary diagram in Figure 2 (left) shows the glass compositions produced in both the anhydrous and H_2O-saturated experiments recalculated from weight percent oxides to mineral components (Ol-Cpx-Pl-SiO_2), using the scheme of Tormey et al. (1987), and projected from Ol onto the Pl-Cpx-SiO_2 plane. The projection from Ol was chosen because all of the hydrous experiments are olivine saturated, and this projection shows compositional variations caused by crystallization of both clinopyroxene and plagioclase. Experimentally determined phase boundaries are shown as dotted (1 atm, anhydrous) and dashed (2 kbar, H_2O-saturated) curves. The most pronounced effect of high H_2O content on phase relations is a shift of the Ol+ Pl + Cpx saturation boundary toward the Pl corner of the pseudo-ternary.

The Pl-Cpx-Ol pseudo-ternary in Figure 2 (right) shows the experimentally produced glass compositions projected from SiO_2 onto the Pl-Cpx-Ol plane. The projection from silica is advantageous because the Ol + Cpx + Pl boundary is nearly perpendicular to the Ol-Cpx-Pl plane, pointing toward the silica apex, and so this boundary projects as a point. A shift of the Ol + Cpx + Pl saturation boundary toward the Pl apex is evident, similar in magnitude to that recognized by Sisson and Grove (1993a) in both natural and simple (Fo-Di-An-H_2O) systems. The present experiments define the position of the Ol + Cpx saturation boundary at 2 kbar, H_2O-saturated. Materials balance calculations of experiments saturated with an assemblage of olivine + high-Ca clinopyroxene (+ chromian spinel) were used to estimate the proportions of pyroxene and olivine that crystallize as the melt evolves along the Ol + Cpx saturation boundary. Calculations

were performed using the glass composition from a high-temperature experiment (e.g., Experiment #12 at 1050°C) with the glass and mineral compositions from a lower temperature experiment (Experiment #7 at 1035°C) (Bryan et al., 1969). The resulting ratio of olivine to pyroxene approximates the proportion of minerals that would be removed from the melt during a process approaching fractional crystallization. The proportion of pyroxene to olivine calculated using this method is ~78:22, a ratio that shows little variation among the three experiments. This is an indication that the Ol + Cpx boundary has very little curvature over this part of composition space.

Comparison of Experimental Results with Lavas from Arcs and Backarcs

Perfit et al. (1980), among others, suggest that an interval of olivine + high-Ca clinopyroxene (± chromian spinel) crystallization, such as that produced in our H_2O-saturated experiments, is important in the evolution of primitive arc-related magmas during crystallization differentiation. Early fractional crystallization of MORB is controlled primarily by olivine and plagioclase fractionation leading to, for example, a positive correlation between MgO and Al_2O_3. Primitive IAB commonly show an increase in Al_2O_3 with decreasing MgO, as in the lavas recovered from Hole 839B and our 2-kbar experiments. This indicates that plagioclase crystallization is suppressed, and the early stages of fractional crystallization are dominated by ferromagnesian silicates. Sisson and Grove (1993b) modeled the crystallization of high-MgO Aleutian basalts to produce low-MgO high-alumina basalts, and found that it required crystallization of high-Ca pyroxene and olivine in approximate proportions 85:15, before plagioclase saturation. Lavas containing high-Ca clinopyroxene and olivine in the approximate volume proportions 75:25 (arc ankaramites) have been reported from Merelava and Epi volcanoes in the Vanuatu arc by Barsdell (1988) and Barsdell and Berry (1990), respectively. Merelava Volcano is located at the southern end of the Northern Trough, a young backarc basin, whereas Epi is located along the volcanic front (Dubois et al., 1978). Table 5 compares the composition of Sample 135-839B-15R-2, 63–67 cm, the starting material for our melting experiments, with whole-rock and groundmass analyses of the most primitive lavas from Merelava (BC 13) and Epi (71046). All three lavas display similar depletions in TiO_2, Al_2O_3 and Na_2O, and high K_2O. The Vanuatu lavas display crystallization sequences similar to that produced in our H_2O-saturated experiments, with early crystallization of high-Ca clinopyroxene and olivine, followed by an assemblage consisting of olivine, high-Ca clinopyroxene, and plagioclase. The chemistry of phenocrysts in these lavas is comparable with those produced in our 2-kbar experiments, with Wo-rich high-Ca clinopyroxene ($Wo_{46.5}En_{50}Fs_{3.5}$ to $Wo_{38}En_{45}Fs_{17}$ from Merelava; $Wo_{47}En_{47.2}Fs_{5.8}$ to $Wo_{44.9}En_{43.8}Fs_{11.3}$ from Epi), and An-rich plagioclase (An_{91} from Merelava; $An_{94.6}$ from Epi). These similarities are evidence that the Vanuatu lavas underwent crystallization in the crust with high pre-eruptive H_2O contents (2–4 wt%).

Comparison of Experimental Results with Lavas Recovered from Hole 839B

The pseudo-ternary diagrams in Figure 3 compare the whole-rock compositions of lavas recovered from Hole 839B with experimentally determined phase boundaries. The lavas have been divided into three groups, based on MgO content. High-MgO lavas (~14 wt%; squares) include Units 3, 4, and 6; medium-MgO lavas (~9 wt%; triangles) are from Unit 1; and low-MgO lavas (~4.5 wt%; circles) include Units 2, 5, 7, and 9. No simple stratigraphic relationship exists between lava MgO content and position in the drill core. Medium MgO lavas are on top, high MgO in the middle, and low MgO are at the base of Hole 839B (Parsons, Hawkins, Allan, et al., 1992). This indicates that a direct relationship between the three groups through fractional crystallization is unlikely, but it does not preclude the possibility that the

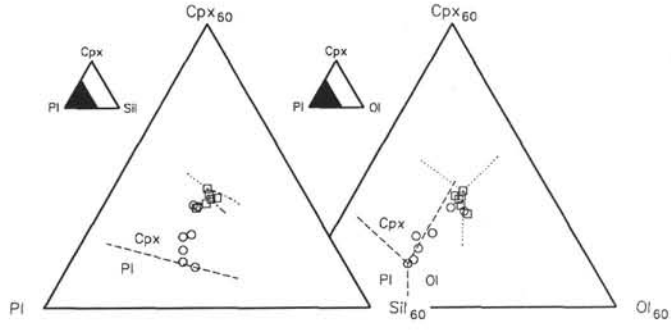

Figure 2. Glass compositions from anhydrous (squares) and water-saturated (circles) experiments recalculated into mineral components (Ol-Cpx-Pl-SiO_2), using the scheme of Tormey et al. (1987), and projected from Ol onto the Pl-Cpx-SiO_2 pseudo-ternary (left) and from SiO_2 onto the Pl-Cpx-Ol pseudo-ternary (right). Experimentally determined phase boundaries are shown as dotted (1 atm, anhydrous) and dashed (2 kb, H_2O-saturated) curves.

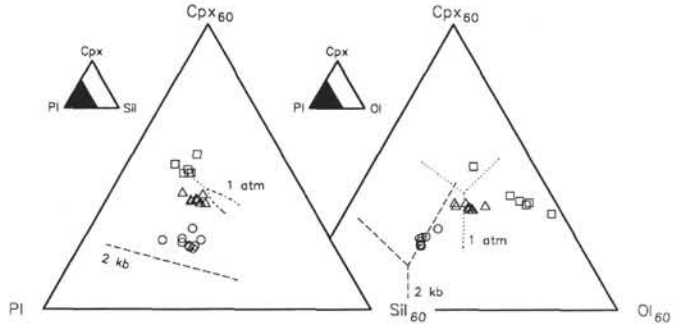

Figure 3. Comparison of Hole 839B lavas with experimentally determined phase boundaries in the projection from Ol onto the Pl-Cpx-SiO_2 pseudo-ternary (left) and from SiO_2 onto the Pl-Cpx-Ol pseudo-ternary (right). Lavas are divided into three groups: high-MgO (~14 wt%; squares), medium-MgO (~9 wt%; triangles) and low-MgO (~4.5 wt%; circles).

parent for the low MgO lavas was similar in composition to the medium or high MgO samples.

Interpreting the compositional variations for a suite of lavas based on analyses of whole rocks is often complicated by the effects of crystal accumulation. This is especially true for lavas with arc affinities, given that they frequently contain a significant proportion of phenocrysts (up to ~50 vol%). Only in cases where crystals have been retained in the proportions in which they crystallized from the magma does the whole-rock composition of a phyric lava represent a liquid. The compositions of lavas from Hole 839B show a general decrease in Cpx component with decreasing MgO content in the projection from Ol onto the Pl-Cpx-SiO_2 pseudo-ternary (Fig. 3; left). Overprinting this trend is a scattering of the data in the direction of the silica apex. A decrease in both Cpx and Ol components with decreasing MgO is evident in the Pl-Cpx-Ol pseudo-ternary (Fig. 3; right), overprinted by scattering toward the Ol apex. These correlations indicate that olivine and high-Ca clinopyroxene are controlling variations in lava compositions, and may be interpreted as either crystallization along the Ol + Cpx boundary or as accumulation of olivine or olivine + high-Ca clinopyroxene crystals.

Figure 4 compares analyses of the glassy chill margins of pillows, which represent liquid compositions, from lavas from Units 3, 4, 6 (high-MgO), 2, and 9 (low-MgO) (Hergt and Nilsson, this volume) with our experimentally determined phase boundaries, and the fields of whole-rock compositions. The glass compositions from the high-MgO lavas (squares) define a trend consistent with crystallization along the 2 kbar, H_2O-saturated experimentally determined Ol + Cpx

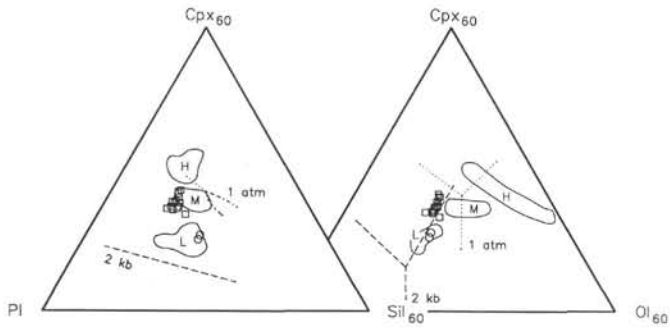

Figure 4. Comparison of analyses of glassy pillow rinds from high-MgO (squares) and low-MgO (circles) lavas from Hole 839B (Hergt and Nilsson, this volume) with experimentally determined phase boundaries and lava whole-rock compositions (H = high-MgO, M = medium MgO, and L = low-MgO) in the Pl-Cpx-SiO_2 (left) and Pl-Cpx-Ol (right) pseudo-ternaries.

saturation boundary. The field of high-MgO whole-rock compositions are enriched in Ol and Cpx, relative to the glasses, and define a trend indicating strong olivine control. Xenocrysts of olivine (Fo_{90}) and chromian spinel have been identified in Unit 3 lavas (Bryan et al., this volume). We propose that the high-MgO lavas represent liquids saturated with olivine and high-Ca clinopyroxene that have been affected by accumulation of olivine and chromian spinel.

To test this model, we first calculated a probable parent magma for the high-MgO lavas, based on the results of our 2-kbar, H_2O-saturated experiments, and then performed mass balance calculations involving the calculated parent, high-MgO lavas and xenocrystic olivine and chromian spinel compositions from Bryan et al. (this volume). The parent composition was calculated by "back fractionating" the glass composition from Experiment #12 (1050°C; Table 3) along the Ol + Cpx saturation boundary, initially using the compositions of the experimentally produced high-Ca pyroxene and olivine. These phases were added to the melt in the constant proportions 78:22, and their compositions were adjusted to be in equilibrium with the melt composition, based on the experimentally determined exchange K_D's, after every 2% addition. The calculations were continued until the melt was in equilibrium with Fo_{89} olivine, which required the addition of 35% crystals. The resulting parent composition is as follows:

SiO_2	TiO_2	Al_2O_3	FeO	MgO	CaO	Na_2O	K_2O
53.10	0.57	13.18	7.70	11.20	12.70	1.22	0.23

The mass balance calculations involving this liquid and the xenocrystic olivine and chromian spinel compositions indicate that the range of observed high-MgO compositions can be generated by addition of the 5–16 wt% Fo_{90} olivine and 3–4 wt% chromian spinel to the inferred high-MgO parent (Table 6).

The whole-rock analyses of the medium-MgO lavas plot close to the glass analyses and are therefore interpreted to be close to liquid compositions. Our 2-kbar experiments on Sample 135-839B-15R-2, 63–67 cm, a medium-MgO lava, produced a few percent crystallization of olivine and chromian spinel before reaching the Ol + Cpx saturation boundary, consistent with minor accumulation of olivine. The field of medium-MgO lava compositions is elongate toward the Ol apex in the Pl-Cpx-Ol pseudo-ternary (Fig. 4; right), evidence consistent with olivine addition, although considerably less olivine addition is required than in the case of the high-MgO lavas. Therefore, we interpret the medium-MgO lavas to represent liquids saturated with olivine and high-Ca pyroxene that have experienced, at most, a few percent addition of olivine (± chromian spinel).

The two available glass analyses from the low-MgO lavas plot in the same area as the whole-rock analyses (Fig. 4), indicating that they have not been significantly affected by crystal accumulation. The low-MgO lavas are displaced toward the 2-kbar, H_2O-saturated boundary, relative to the anhydrous phase boundaries in the Pl-Cpx-SiO_2 pseudo-ternary; and they appear to fall along a Cpx + Pl ± Ol ± Opx saturation boundary (Fig. 3; left). The projected low-MgO lava compositions cluster in a narrow region in the Pl-Cpx-Ol pseudo-ternary (Fig. 3; right) that represents a Cpx + Pl ± Ol ± Opx saturation boundary. This boundary is close to the 2-kbar, H_2O-saturated boundary, but it is displaced slightly toward the 1-atm boundary. Both projections are consistent with the low-MgO lavas crystallizing at ~1.5 kbar, H_2O-saturated, or near 2 kbar at conditions that were not quite H_2O-saturated. The presence of plagioclase phenocrysts with Ca-rich cores (An_{90}) in the low-MgO lavas (Bryan et al., this volume) implies a Ca-Na exchange K_D of ~3.1, a further indication of elevated pre-eruptive H_2O contents in these lavas.

Figure 5 is a schematic, showing the major processes involved in the petrogenesis of Hole 839B lavas. Variable amounts of fractional crystallization along the Ol + Cpx saturation boundary under hydrous conditions, represented by the solid curves in both the Pl-Cpx-SiO_2 (left) and Pl-Cpx-Ol (right) pseudo-ternaries, produced a spread in the lavas from high-MgO (field labeled H) through medium- (field labeled M) to low-MgO (field labeled L) lavas. The accumulation of olivine and chromian spinel caused a spread within high- and medium-MgO lava compositions toward the Ol apex of the Pl-Cpx-Ol pseudo-ternary. The low-MgO lavas have reached plagioclase saturation, and possibly the olivine-out reaction point, and evolved along the Cpx + Pl ± Ol ± Opx saturation boundary (solid curve labeled Cpx + Pl ± Ol ± Opx in the Pl-Cpx-Ol pseudo-ternary).

The compositions of high-Ca pyroxene and plagioclase phenocrysts analyzed in Unit 1 (medium-MgO) lavas are consistent with high pre-eruptive H_2O contents. The high-Ca clinopyroxenes analyzed in Samples 135-839B-15R-3, 72–76 cm, and 135-839B-14R-2, 1–8 cm, are close in composition to those produced in our 2-kbar, H_2O-saturated experiments (Tables 3–4 and Fig. 1), with ~20 wt% CaO, whereas the 1-atm, anhydrous experiments produced augites

Table 5. Comparison of Sample 135-839B-15R-2, 63–67 cm, with whole-rock and groundmass analyses of similar lavas from Merelava (Barsdell, 1988) and Epi (Barsdell and Berry, 1990) in the Vanuatu arc.

	Sample 135-839B-15R-2, 63–67 cm	BC 13	BC 13 groundmass	71046	71046 groundmass
SiO_2	53.3(2)	50.2	50.8	48.2	48.2
TiO_2	0.60(3)	0.46	0.71	0.39	0.67
Al_2O_3	15.16(8)	10.3	15.2	11.5	16.2
FeO*	8.85(8)	8.09	9.00	8.91	9.81
MnO	0.22(2)	0.17	0.16	0.16	0.16
MgO	9.36(5)	13.71	8.82	13.50	8.00
CaO	11.3(1)	13.69	11.8	14.4	13.3
Na_2O	1.48(5)	1.6	2.09	1.05	1.88
K_2O	0.30(2)	0.38	0.48	0.31	0.48
Total	100.57	98.60	99.06	98.42	98.70

Table 6. Least-squares mass balance models relating calculated parent magma composition with high-MgO lava whole-rock compositions through accumulation of olivine and chromian spinel.

High-MgO lava sample	Parent (wt%)	Olivine (wt%)	Chromian spinel (wt%)	ΣR^2
135-839B-				
27R-1, 21–24 cm	90.99	5.51	3.15	0.6444
19R-1, 50–56 cm	90.45	6.46	3.13	0.3192
23R-1, 22–27 cm	88.42	7.75	3.85	0.2006
20R-1, 74–80 cm	87.51	8.80	3.59	0.1092
24R-1, 14–19 cm	81.23	15.93	2.80	0.5577

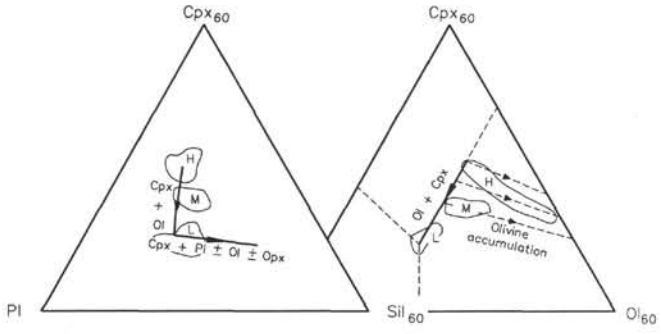

Figure 5. Schematic diagram showing the major processes involved in the petrogenesis of Hole 839B lavas, in the Pl-Cpx-SiO_2 (left) and Pl-Cpx-Ol (right) pseudo-ternaries. Heavy arrowed lines indicate fractional crystallization. Dashed arrowed lines indicate crystal accumulation. Inferred phase boundaries are shown as dashed lines. Fields of lava whole-rock compositions are labeled as in Figure 4.

with only ~18 wt% CaO (Table 2). The cores of plagioclase phenocrysts from these samples are consistently An-rich (An_{89} in Sample 135-839B-15R-3, 72–76 cm, and An_{91} in Sample 135-839B-14R-2, 1–8 cm). This indicates a Ca-Na exchange K_D of ~2, assuming that crystal accumulation has not affected the whole-rock Ca/Na ratio. A K_D of 2 indicates ~2 wt% H_2O, based on the experiments of Baker and Eggler (1987). The simplest explanation for the observations of coexisting olivine + high-Ca clinopyroxene phenocrysts, minor An-rich plagioclase rimmed by more Na-rich plagioclase, and orthopyroxene cored by olivine is that the magma was initially H_2O rich (~4–5 wt%), and it underwent at least two episodes of volatile loss. The initial change in volatile content stabilized a minor amount of An-rich plagioclase, producing the assemblage found in Sample 135-839B-15R-3, 72–76 cm. Crystallization along the Ol + Cpx + Pl boundary over any significant temperature interval would have produced more plagioclase than is present in thin section and is therefore unlikely. Further volatile loss, caused by low-pressure crystallization, stabilized orthopyroxene relative to olivine, less calcic augite, and a more albite-rich plagioclase, producing the assemblage observed in Sample 135-839B-14R-2, 1–8 cm.

CONCLUSIONS

On the basis of natural and experimental evidence, we conclude that the chemical variations in Hole 839B lavas result primarily from hydrous fractional crystallization at crustal level pressures. A positive correlation between Al_2O_3 and SiO_2, which distinguishes these back-arc lavas from others recovered during Leg 135, results from the suppression of plagioclase crystallization caused by high pre-eruptive H_2O contents. The dominant control on melt composition is crystallization, under hydrous conditions, of high-Ca clinopyroxene and olivine in approximately 78:22 proportions; evidence also exists for variable amounts of olivine and chromian spinel accumulation. Low-MgO lavas from Hole 839B likely evolved through crustal level fractional crystallization, under hydrous conditions, from a parent similar to basaltic andesite Sample 135-839B-15R-2, 63–67 cm.

Lavas from Hole 839B are estimated to have had pre-eruptive H_2O contents of ~4 wt%. The medium-MgO lavas underwent an episode of volatile loss, decreasing their H_2O content to ~2 wt% and stabilizing orthopyroxene and plagioclase phenocrysts. This loss of volatiles may have accompanied ascent of the magma into the shallow crust just before eruption.

ACKNOWLEDGMENTS

The authors thank Dave Walker and Roger Nielsen for reviews, and Kristin Nilsson for advance access to Hole 839B glass analyses. This research was supported by NSF grants OCE-9115901 and EAR-9204661. Mike Jercinovic expertly maintained the MIT electron microprobe facility where the phenocrysts and experimental run products where analyzed.

REFERENCES*

Albee, A.L., and Ray, L., 1970. Correction factors for electron microprobe analysis of silicates, oxides, carbonates, phosphates and sulfates. *Anal. Chem.*, 42:1408–1414.

Baker, D.R., and Eggler, D.H., 1987. Compositions of anhydrous and hydrous melts coexisting with plagioclase, augite and olivine or low-Ca pyroxene from 1 atm to 8 kbar: applications to the Aleutian volcanic center of Atka. *Am. Mineral.*, 72:12–28.

Barsdell, M., 1988. Petrology and petrogenesis of clinopyroxene-rich tholeiitic lavas, Merelava Volcano, Vanuatu. *J. Petrol.*, 29:927–964.

Barsdell, M., and Berry, R.F., 1990. Origin and evolution of primitive island arc ankaramites from western Epi, Vanuatu. *J. Petrol.*, 31:747–777.

Bence, A.E., and Albee, A.L., 1968. Empirical correction factors for the electron microanalysis of silicates and oxides. *J. Geol.*, 76:382–403.

Biggar, G.M., 1972. Diopside, lithium metasilicate and the 1968 temperature scale. *Mineral. Mag.*, 38:768–770.

Bryan, W.B., Finger, L.W., and Chayes, F., 1969. Estimating proportions in petrographic mixing equations by least squares approximations. *Science*, 163:926–927.

Dubois, J., Dugas, J., Lapouille, A., and Louat, R., 1978. The troughs at the rear of the New Hebrides Island arc: possible mechanisms of formation. *Can. J. Earth Sci.*, 15:351–360.

Gill, J.B., 1981. *Orogenic Andesites and Plate Tectonics:* New York (Springer-Verlag).

Grove, T.L., 1981. Use of FePt alloys to eliminate the iron loss problem in 1 atmosphere gas mixing experiments: theoretical and practical considerations. *Contrib. Mineral. Petrol.*, 78:298–304.

Grove, T.L., and Baker, M.B., 1984. Phase equilibrium controls on the tholeiitic versus calc-alkaline differentiation trends. *J. Geophys. Res.*, 89:3253–3274.

Grove, T.L., and Bryan, W.B., 1983. Fractionation of pyroxene-phyric MORB at low pressure: an experimental study. *Contrib. Mineral. Petrol.*, 84:293–309.

Grove, T.L., Kinzler, R.J., and Bryan, W.B., 1990. Natural and experimental phase relations of lavas from Serocki Volcano. *In* Detrick, R., Honnorez, J., Bryan, W.B., Juteau, T., et al., *Proc. ODP, Sci. Results,* 106/109: College Station, TX (Ocean Drilling Program), 9–17.

Hart, S.R., Glassley, W.A., and Karig, D.E., 1972. Basalts and seafloor spreading behind the Mariana Island arc. *Earth Planet. Sci. Lett.*, 15:12–18.

Parson, L., Hawkins, J., Allan, J., et al., 1992. *Proc. ODP, Init. Repts.*, 135: College Station, TX (Ocean Drilling Program).

Perfit, M.R., Gust, D.A., Bence, A.E., Arculus, R.J., and Taylor, S.R., 1980. Chemical characteristics of island-arc basalts: implications for mantle sources. *Chem. Geol.*, 30:227–256.

Poldervaart, A., and Hess, H.H., 1951. Pyroxenes in the crystallization of basaltic magma. *J. Geol.*, 59:472–489.

Roeder, P.L., and Emslie, R.F., 1970. Olivine-liquid equilibrium. *Contrib. Mineral. Petrol.*, 29:275–289.

Sisson, T.W., and Grove, T.L., 1993a. Experimental investigations of the role of H_2O in calc-alkaline differentiation and subduction zone magmatism. *Contrib. Mineral. Petrol.*, 113:143–166.

———, 1993b. Temperatures and H_2O contents of low-MgO high-alumina basalts. *Contrib. Mineral. Petrol.*, 113:167–184.

Tormey, D.R., Grove, T.L., and Bryan, W.B., 1987. Experimental petrology of normal MORB near the Kane Fracture Zone: 22°–25°N, Mid-Atlantic Ridge. *Contrib. Mineral. Petrol.*, 96:121–139.

*Abbreviations for names of organizations and publication titles in ODP reference lists follow the style given in *Chemical Abstracts Service Source Index* (published by American Chemical Society).

Date of initial receipt: 30 June 1992
Date of acceptance: 3 December 1992
Ms 135SR-133